JHEP

Published by Institute of Physics Publishing for SISSA

Received: *December 20, 2005*
Revised: *January 31, 2006*
Accepted: *February 1, 2006*
Published: *February 14, 2006*

Parton distributions and the strong coupling: CTEQ6AB PDFs

Jon Pumplin, Alexander Belyaev, Joey Huston, Daniel Stump and Wu-Ki Tung

Department of Physics and Astronomy, Michigan State University
E. Lansing, MI 48824, U.S.A.
E-mail: pumplin@pa.msu.edu, belyaev@pa.msu.edu, huston@pa.msu.edu, stump@pa.msu.edu, tung@pa.msu.edu

Abstract: We study the global analysis for parton distributions as a function of the QCD strong coupling strength α_s, and present a new series of distributions that span the range $0.110 < \alpha_s(m_Z) < 0.128$. We use these distributions to explore the correlation between α_s and the gluon distribution; the viability of global analysis as a method to measure α_s; and the dependence on α_s of predictions for W, Z, inclusive jet, and Higgs boson production ($b\bar{b} \to H$ and $gg \to H$) cross sections at the Tevatron and the LHC. We find that the uncertainty in α_s is the dominant source of uncertainty for inclusive jet production at moderately small p_T and for Higgs production at intermediate masses in the Standard Model.

Keywords: QCD, Deep Inelastic Scattering, Hadronic Colliders, Parton Model.

JHEP02(2006)032

Contents

1. Introduction

The theory of Quantum Chromodynamics (QCD) depends on the fundamental gauge coupling strength α_s and suitably defined quark mass parameters m_f. For applications to hard scattering processes with hadrons in the initial state, we also need the universal parton distribution functions (PDFs) that characterize the partonic structure of those hadrons. These PDFs are determined by global QCD analysis, using input from a variety of well-established experimental measurements.

In the standard CTEQ analysis [1], the focus is on determining the parton distribution functions. The value of $\alpha_s(m_Z)$ is fixed at the world average value, which is dominantly based on dedicated measurements such as those from LEP, where it was determined in processes that are free of the complications of hadronic structure.

However, the interplay between the coupling strength α_s and strong dynamics is an interesting subject in itself. Many attempts have been made to extract $\alpha_s(m_Z)$ from individual experiments at the HERA ep collider, at the Tevatron $p\bar{p}$ collider, and from combined analyses of several hadronic experiments. For such studies, as well as to assess the additional uncertainty in predictions caused by the uncertainty in $\alpha_s(m_Z)$, it is important to have PDF sets available that are based on a range of different values for α_s. The purpose of this paper is to fill that need.

We provide here a series of PDF sets that span a range of coupling strengths from $\alpha_s(m_Z) = 0.110$ to 0.128. These PDFs extend and update the CTEQ6 global analysis [1].

JHEP02(2006)032

They are successors to the α_s series that was determined in the CTEQ4 analysis [2]. Complementary to the physics probed in [1], we will discuss several issues related to the dependence on α_s: the correlation between α_s and the parton distributions — particularly the gluon distribution; the viability of using global analysis of hadronic processes to measure α_s; and the dependence on α_s of physics predictions for W, Z, jet, and Higgs boson cross sections at the Tevatron and the Large Hadron Collider LHC.

We provide two different sets of fits — CTEQ6A and CTEQ6B — corresponding to two different common definitions for $\alpha_s(\mu)$ that are defined in the next section.

2. Definitions for $\alpha_s(\mu)$

The dependence of the QCD coupling strength $\alpha_s(\mu)$ on the momentum scale μ is governed by the renormalization group equation (RGE), which in next-to-leading order (NLO) perturbation theory is

$$\mu\, d\alpha/d\mu = c_1\alpha^2 + c_2\alpha^3 \,, \tag{2.1}$$

where $c_1 = -\beta_0/2\pi$ with $\beta_0 = 11 - (2/3)\mathrm{n}_f$, and $c_2 = -\beta_1/8\pi^2$ with $\beta_1 = 102 - (38/3)\mathrm{n}_f$. The coefficients are functions of the number of active quark flavors n_f. These coefficients change discontinuously as μ passes the mass m_f of each quark flavor and the integer n_f jumps up by 1; nevertheless at NLO, the function $\alpha_s(\mu)$ is a *continuous* function of μ at these thresholds. The solution to eq. (2.1) therefore depends on a single integration constant, which is the fundamental coupling strength parameter of QCD that is usually chosen to be $\alpha_s(m_Z)$.

Since eq. (2.1) is truncated at $\mathcal{O}(\alpha^3)$, there are infinitely many definitions of $\alpha_s(\mu)$ that are formally equivalent because they differ only in higher orders of the perturbative expansion. Two choices that are often used in QCD phenomenology are:

- **Def. A.** The original NLO definition [3] is given by

$$\alpha_s(\mu) = c_3\,[1 - c_4\ln(L)/L]/L \,, \tag{2.2}$$

  where $L = \ln(\mu^2/\Lambda^2)$, $c_3 = -2/c_1$, and $c_4 = -2\,c_2/c_1^2$. The parameter Λ depends on n_f, and hence takes on different values Λ_{n_f} when μ crosses each quark mass threshold. Previous CTEQ global analyses have all used this definition for the running coupling.

- **Def. B.** An alternative is to solve the truncated RGE (2.1) exactly. The publicly available evolution program QCDNUM [4], and many HERA analyses use this definition.

We have shown previously [5] that these two forms are numerically quite similar in the region $Q > 2\,\mathrm{GeV}$ where we fit data. In the following, we present results based on both definitions,[1]

[1] The form used for PDF fitting by MRST [6] is different from both of these definitions, but is numerically very close to Def. B [5]. The definition used by the Particle Data Group [7] lies between Def. A and Def. B.

3. The CTEQ6 α_s series of global fits

To study the interplay between the strong coupling strength α_s and the PDFs, one can either perform a fully global QCD fit by varying α_s and the PDF parameters simultaneously to examine the neighborhood of the overall global minimum in χ^2; or one can perform a series of fits to the PDF parameters at various fixed values for α_s. We have explored both of these approaches, but concentrate here on the second approach since it is most convenient for general collider physics applications. We therefore present here a series of PDFs — the CTEQ6 α_s-series. Some of their physical implications are discussed in section 6. Earlier PDF fits with a range of $\alpha_s(m_Z)$ have been obtained in [2, 8]. Fits with a range of $\alpha_s(m_Z)$ and their interplay with the gluon distribution were studied in connection with the possibility of coevolution with light gluinos in [9].

The PDFs in the new series were obtained for 10 values of $\alpha_s(m_Z) = 0.110$, 0.112, ..., 0.128, where $m_Z = 91.188\,\text{GeV}$ is assumed. The theoretical assumptions and functional parametrization of these PDFs at the initial momentum scale $\mu_0 = 1.3\,\text{GeV}$ are the same as in the previous CTEQ6 analysis [1, 10]. The experimental input is slightly updated.[2] These PDF sets are designated as CTEQ6A110, ..., CTEQ6A128 using Def. A for α_s; and CTEQ6B110, ..., CTEQ6B128 using Def. B for α_s. The fits CTEQ6A118 and CTEQ6B118, which have $\alpha_s(m_Z) = 0.118$, are nearly the same as CTEQ6M or CTEQ6.1M, but are not identical to either due to minor updates in experimental input, and in the case of CTEQ6B118 the different definition for α_s. All 20 of these PDF sets will give very similar physical predictions for most applications.

Figure 1 shows the quality of the global fits, as measured by the overall χ^2 for the fit to $\sim$2000 data points, as a function of $\alpha_s(m_Z)$.[3] The two curves, both approximately parabolic, are smooth interpolations of the above series of fits. The curves are very similar, with the Def. A curve being slightly narrower and slightly farther to the left because Def. A has a little more rapid variation of $\alpha_s(\mu)$ with μ. The minima of these curves are at $\alpha_s(m_Z) = 0.1172$ and 0.1176, close to the current world average (0.1187 ± 0.0020) [7] and very close to the value 0.1180 used in CTEQ6M and CTEQ6.1M. This similarity in α_s is an impressive demonstration of consistency between QCD theory and experiment, since the global QCD analysis is based on hard scattering data with hadronic initial states, while the determination of the world average value for α_s comes mainly from totally different physical processes such as e^+e^- annihilation, τ-decay, and even lattice gauge theory calculations with quarkonium spectra as input.

Note that the range of $\alpha_s(m_Z)$ covered by the CTEQ6AB series is much wider than the currently accepted 1σ error range of the world average quoted above. We explore this extended range because the lowest and highest values (0.110, 0.128) represent outlying

[2] The input experimental data consist of BCDMS (muon F_2 on hydrogen and deuterium) [11], H1 ($e^\pm$ F_2) [12], ZEUS ($e^\pm$ F_2) [13], NMC (muon F_2 on hydrogen and deuterium) [14], CCFR (neutrino F_2 and xF_3 on iron) [15], E866 (Drell-Yan muon pairs from *pp* and *pd*) [16], CDF (W-lepton asymmetry) [17], CDF (inclusive jet) [18] and D0 (inclusive jet) [19]. The update consists mainly of including the data from the first of the three references in [12] which was inadvertently omitted in CTEQ6.

[3] This figure is an improved version of one appearing in [5].

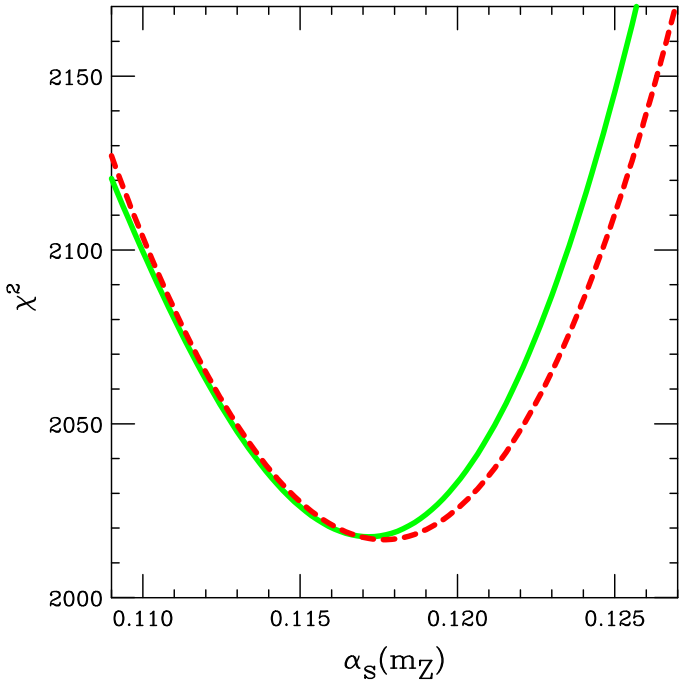

Figure 1: The overall goodness-of-fit measure χ^2 for global fits vs. $\alpha_s(m_Z)$, using Def. A (solid curve) and Def. B (dashed curve).

values that have been obtained by some individual experiments that are included in the world average. The fits with extreme values of $\alpha_s(m_Z)$ will be useful for some specialized applications. In plots shown later in this paper, we show almost all of this range, but reduce it to 0.110 to 0.126 to be symmetric about the CTEQ6 value of 0.118. Note that χ^2 increases by ~ 100 above its minimum at the extremes of this reduced range, which makes it consistent with a 90% confidence range for the global fit according to results of our previous analyses. However, the reader must keep in mind that this range of $\alpha_s(m_Z)$ is larger by a factor of $\sim$4 than the uncertainty range corresponding to a "1σ" error band based on the world average data.

4. The gluon distribution and α_s

The gluon distribution is strongly correlated with α_s in the global QCD analysis. This can be seen in figure 2(a), which shows the gluon distributions $g(x, \mu)$ from the α_s-series PDFs as a function of momentum fraction x at scale $\mu = 3.162\,\text{GeV}$ ($\mu^2 = 10\,\text{GeV}^2$). For clarity of display, the horizontal axis is scaled as $x^{1/3}$ and the vertical axis is weighted by $x^{3/2}$.

For comparison, figure 2(b) shows the uncertainty band (shaded area) of the gluon distribution due to sources other than α_s. This uncertainty was computed at a fixed value $\alpha_s(m_Z) = 0.118$ by the Hessian method [20], using the 40 eigenvector basis sets of CTEQ6.1 [10]. The CTEQ6.1M (solid) and the new CTEQ6A118 (dashed) distributions, which are very similar, are also shown in figure 2(b). The two figures are combined in figure 2(c), where, in order to highlight the differences, the results are shown as ratios to the CTEQ6.1M distribution.

JHEP02(2006)032

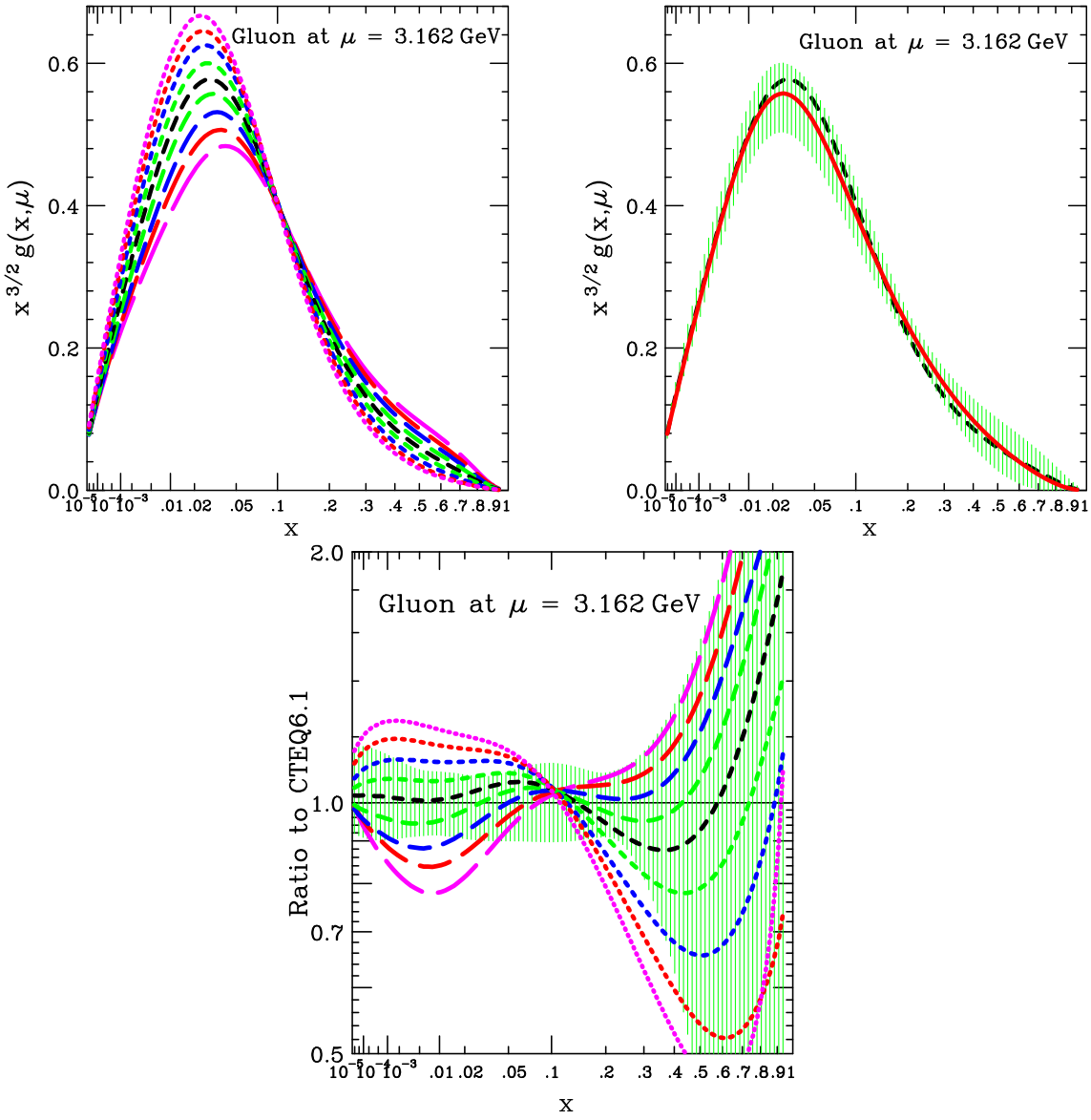

Figure 2: (a) Gluon distributions for CTEQ6A110 (short dash), ..., CTEQ6A126 (long dash). These have $\alpha_s(m_Z) = 0.110$ (short dash), ..., 0.126 (long dash) using Def. A for α_s; (b) Gluon distributions with $\alpha_s(m_Z) = 0.118$: CTEQ6A118 (dashed), CTEQ6.1M (solid), and uncertainty band from CTEQ6.1 eigenvector sets (shaded); (c) Both plots combined in ratio form.

There is a clear systematic trend in the α_s-series for the gluon distribution function. Fits with larger $\alpha_s(m_Z)$ have a gluon component that is weaker at small x and stronger at large x. The behavior at small x results from the fact that every occurrence of $g(x, \mu)$ in a cross section formula is accompanied by a factor of α_s, so when α_s is made larger, the gluon distribution becomes smaller in order to maintain agreement with the large amount of data at small x. The behavior at large x, where the direct experimental constraints on the gluon are weaker, is dictated by the momentum sum rule: the total momentum fraction carried by gluon + quarks must be equal to 1, and the momentum carried by quarks is tightly constrained by DIS data.

JHEP02(2006)032

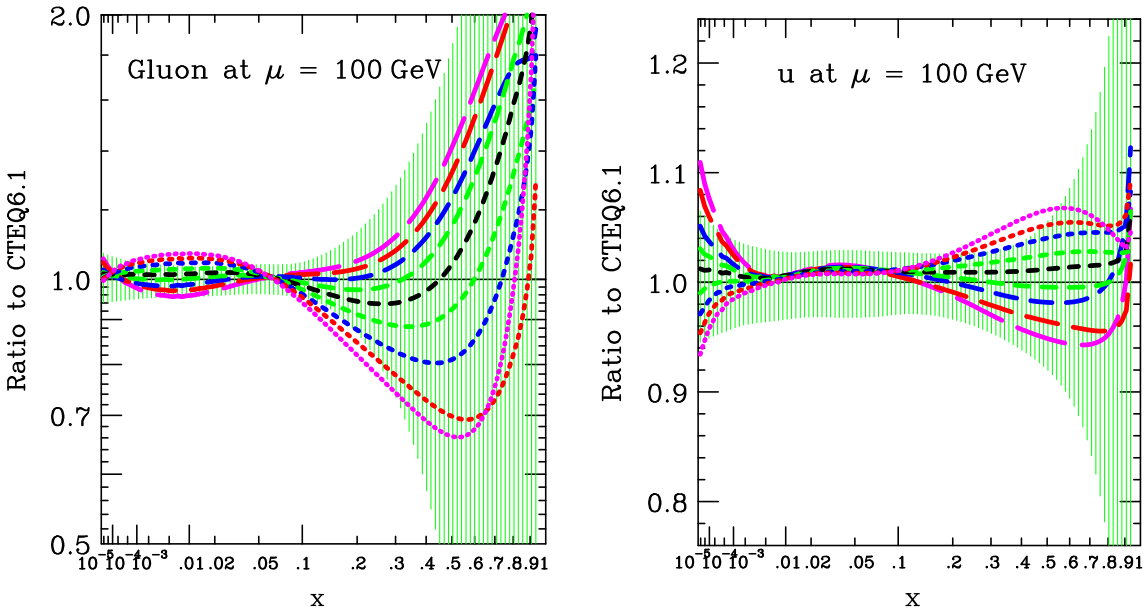

Figure 3: Uncertainties at scale $\mu = 100\,\text{GeV}$ for Gluon (a), and u-quark (b).

Another feature seen in figure 2 is that the gluon distributions for different $\alpha_s(m_Z)$ values all nearly intersect at a common value $x \approx 0.1$. This occurs simply because the function $g(x, \mu, \alpha_s(m_Z))$ varies rather slowly and smoothly with $\alpha_s(m_Z))$, so its dependence on $\alpha_s(m_Z))$ can be approximated rather well by the first order (linear) term of a Taylor series. This linearity can also be seen by the nearly equal spacing of the curves in figure 2(a) and (c).

Comparing the range of variation of $g(x, \mu)$ due to the variation of α_s, to the uncertainty range due to other sources of error, we see that the two are comparable throughout most of the domain in x. The *combined* uncertainty on the gluon distribution is therefore somewhat larger than the previously published uncertainties, which were obtained at fixed $\alpha_s(m_Z)$.

Figure 3(a) shows the gluon uncertainty at $\mu = 100\,\text{GeV}$. At this larger momentum scale, the overall uncertainty is much smaller, and the α_s contribution to the uncertainty is generally smaller than the uncertainty due to the causes that are included in the Hessian analysis. Figure 3(b) similarly shows the uncertainty for the up quark distribution at $\mu = 100\,\text{GeV}$. The uncertainty for the quark is much smaller than for gluon (note the different y-axis in the graph) and again the α_s contribution is small compared to the other sources of uncertainty.

5. Can we determine α_s from the global analysis?

It is natural to try to determine the coupling strength α_s from the global QCD fit to hadronic processes. It appears straightforward to do so, since one can simply treat the parameter $\alpha_s(m_Z)$ as one of the fitting parameters. We see from the minima in figure 1 that

JHEP02(2006)032

the resulting "best fit" value of $\alpha_s(m_Z)$ is around 0.1174, which is very close to the world average value. The difficult question, however, is what uncertainty should be assigned to this measurement. The answer to that question determines whether this method is competitive with measurements that are independent of the complications of hadron partonic structure. The fact that the value of $\alpha_s(m_Z)$ in global analysis is strongly correlated with the rather uncertain gluon distribution, as discussed in the previous section, suggests that caution is needed.

Referring again to figure 1, the range of $\alpha_s(m_Z)$ (horizontal axis) allowed by global analysis based on minimization of χ^2, is set by the increase of χ^2 (vertical axis) above the global minimum that we allow. We refer to the allowed increase of χ^2 as the *tolerance*, $\Delta\chi^2$. Recent studies of uncertainties of PDFs by various global analysis groups [1, 6, 21] have concluded that a reasonable tolerance $\Delta\chi^2$ must be rather large, in the range 50 – 100 for the $\sim$2000 points in present-day data sets, to define an approximate 90% confidence range. Making the specific choice $\Delta\chi^2 = 100$, the corresponding range of $\alpha_s(m_Z)$ is from 0.1093 to 0.1247. Assuming that range to be the 90% confidence range for a gaussian distribution, it corresponds to $\alpha_s(m_Z) = 0.1170 \pm 0.0047$ for a "1σ" error range. Thus the measurement of $\alpha_s(m_Z)$ provided by PDF fitting agrees very well with the Particle Data Group world average of 0.1187 ± 0.0020 [7], but has more than twice its uncertainty. Hence the PDF result cannot be used to substantially reduce the uncertainty in $\alpha_s(m_Z)$ at the present time.

We can gain some insight on how α_s is constrained in the global QCD analysis by examining the dependence on $\alpha_s(m_Z)$ of the χ^2 values for each individual experiment that contributes to that analysis. These χ^2 "parabolas" are shown in figure 4. The curves represent smooth interpolations of the results from the 10 fits in the CTEQA α_s-series. The vertical axis in each graph is the χ^2 value per data point in the fit to that experiment, while the horizontal axis is $\alpha_s(m_z)$.

It is apparent in figure 4 that the sensitivities of the various experiments to α_s vary greatly. Some of the curves are approximately parabolic with a minimum within the range probed, while others merely constrain the value of $\alpha_s(m_Z)$ from above or below. The global minimum seen in figure 1 is due to the combined constraints of all the experiments. Since different experiments prefer different values of $\alpha_s(m_Z)$, which are not always consistent with each other if strict statistical criteria ("$\Delta\chi^2 = 1$") are applied to each experiment, the global minimum represents a compromise that is difficult to interpret as a "measurement" in the traditional sense.[4] In particular, there is no clear way to assign a statistically meaningful error to the measurement. Rather, the error is dominated by systematic effects that can only be estimated.

6. Dependence of predicted cross sections on α_s

Here we present predictions for several important processes at the Tevatron ($\bar{p}p$ at $\sqrt{s} =$

[4]We should point out that the χ^2 curves shown in figure 4 are not to be compared directly to those obtained by individual experiments in their respective determinations of α_s. The points on our curves correspond to χ^2 values evaluated using constrained fits to the full global data set, not just to the data of a single experiment.

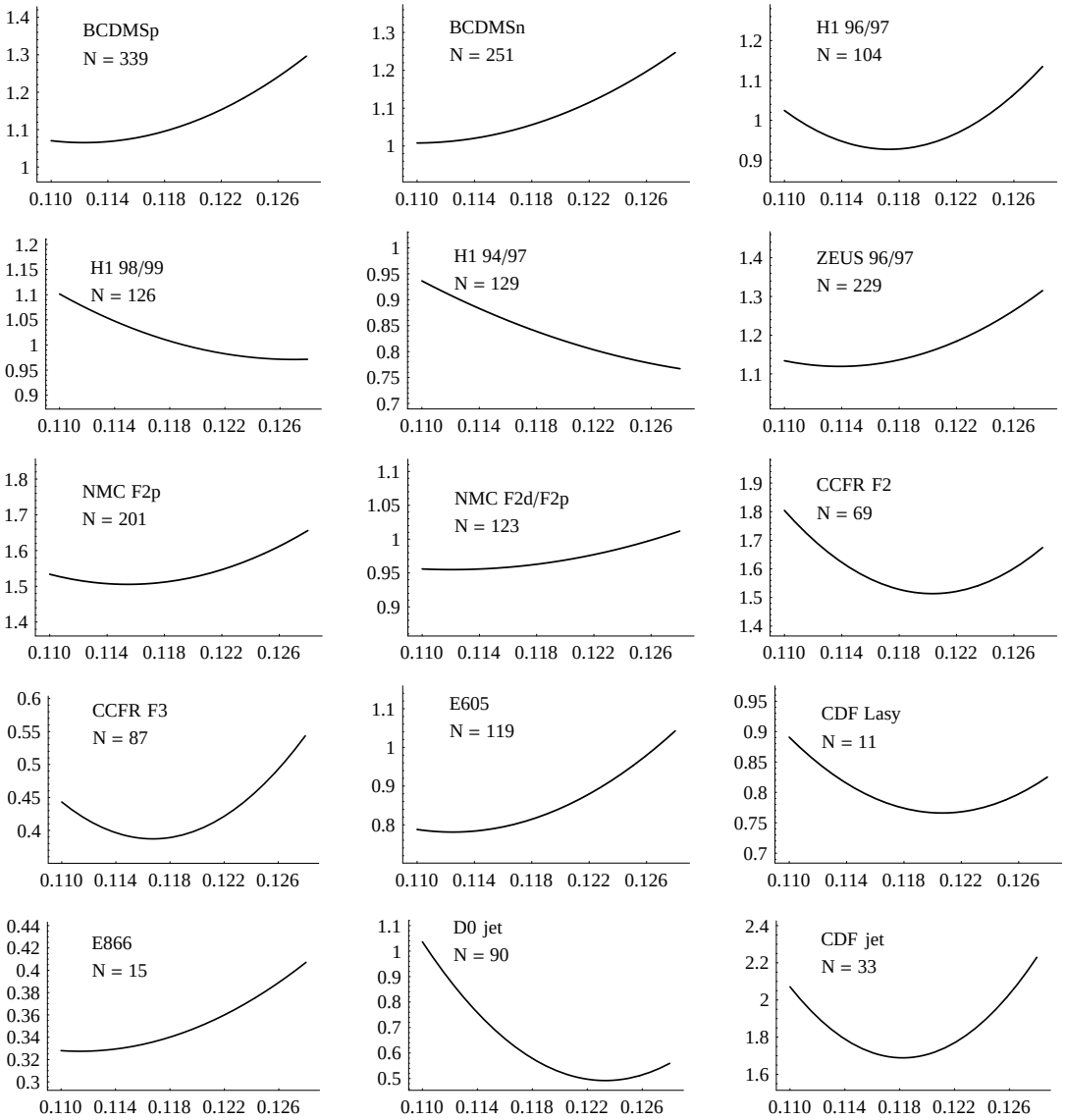

Figure 4: The χ^2 values per data point for the individual experiments that are included in the global analysis, as a function of $\alpha_s(m_Z)$. The number of data points is indicated on each figure.

1.96 TeV) and the LHC (pp at $\sqrt{s} = 14\,\text{TeV}$). The results show how the uncertainty in α_s propagates to uncertainties in physical predictions. At the same time, the results show to what extent accurate measurements of these cross sections could be used to constrain α_s.

We show predictions using the Def. A form for α_s. Results for the Def. B form are very similar. The figures show the variation of the predictions for the range of $\alpha_s(m_Z)$ from 0.110 to 0.126. We again remind the reader that this range is much larger than the actual uncertainty of $\alpha_s(m_Z)$; i.e., the full variation of the physical predictions shown in

JHEP02(2006)032

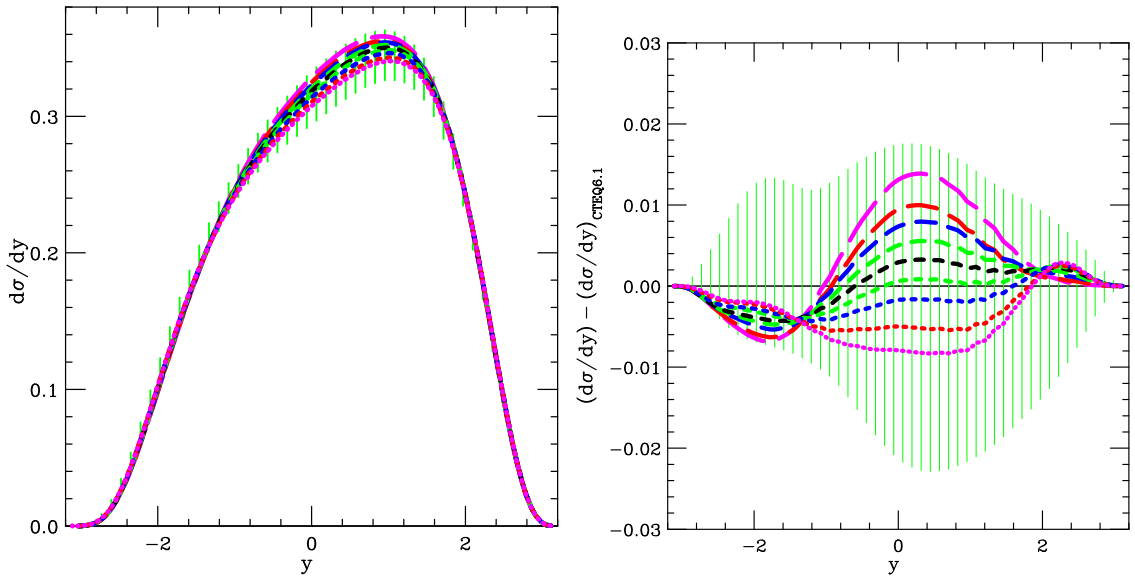

Figure 5: (a) Cross section $d\sigma/dy_W$ for W^- production at the Tevatron. (b) Same cross section with the CTEQ6.1 prediction subtracted. The curves are for $\alpha_s(m_Z) = 0.110$ (short dash), ..., 0.126 (long dash) as in figure 2.

each figure extends beyond the actual uncertainty from α_s. The shaded region in each figure shows the range of uncertainty due to sources other than α_s, as calculated from the eigenvector basis sets of CTEQ6.1 using the Hessian method [10, 20]. These are assumed to estimate the 90% confidence range.

6.1 W and Z production

Figure 5 shows the cross section for W^- production at the Tevatron.[5] W^+ production is identical except for $y \to -y$. The left plot shows $d\sigma/dy_W$ versus the W rapidity y_W. The right plot shows the difference from the prediction of CTEQ6.1, which has $\alpha_s(m_Z) = 0.118$. The curves are the CTEQ6A α_s-series, and the shaded band is the range of uncertainty for fixed $\alpha_s(m_Z)$, calculated using the Hessian method. For this process, the Hessian uncertainty range is about $\pm 5\%$ of the central prediction. The variation with α_s is smaller, on the order of $\pm 2\%$, even for the extreme range of $\alpha_s(m_Z)$ from 0.110 to 0.126.

Figure 6 shows the cross section $d\sigma/dy_Z$ for Z^0 production at the Tevatron. Again the Hessian uncertainty range is $\sim \pm 5\%$ and again the variation with $\alpha_s(m_Z)$ is $\sim \pm 2\%$ for the extreme range of α_s.

Figure 7 shows the cross section for W^- production at the LHC. The Hessian uncertainty range is again of order $\pm 5\%$, but the variation with α_s is larger than for the Tevatron, of order $\pm 5\%$ for the large range of $\alpha_s(m_Z)$ that is shown. Figure 8 shows

[5] All cross sections shown for $W^\pm$ and Z^0 production are given in nanobarns, with the leptonic decay branching fraction included.

JHEP02(2006)032

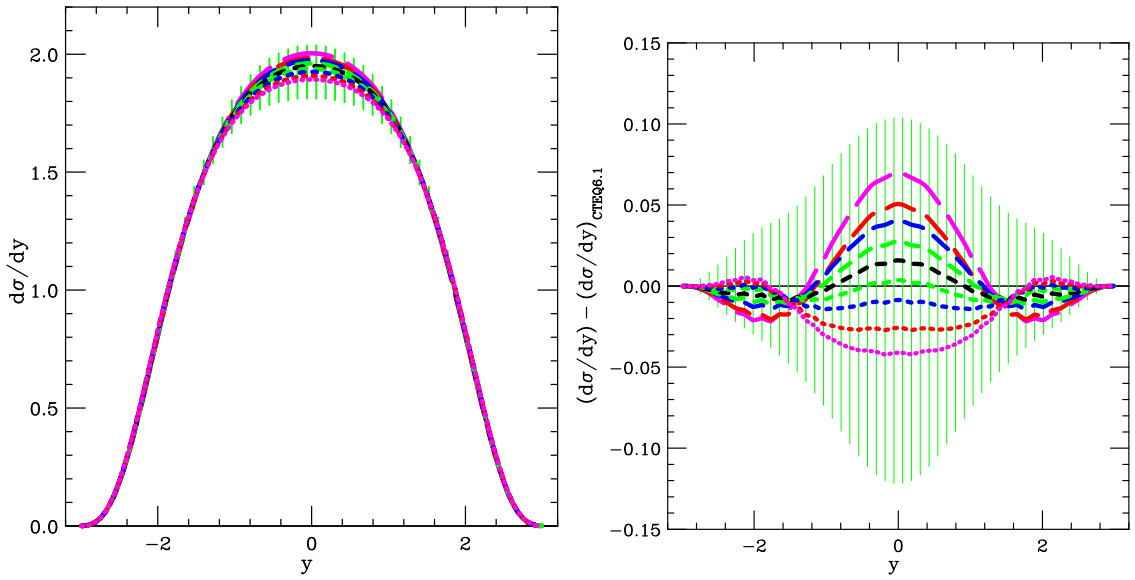

Figure 6: (a) Production of Z^0 at the Tevatron; (b) Same process with the CTEQ6.1 prediction subtracted.

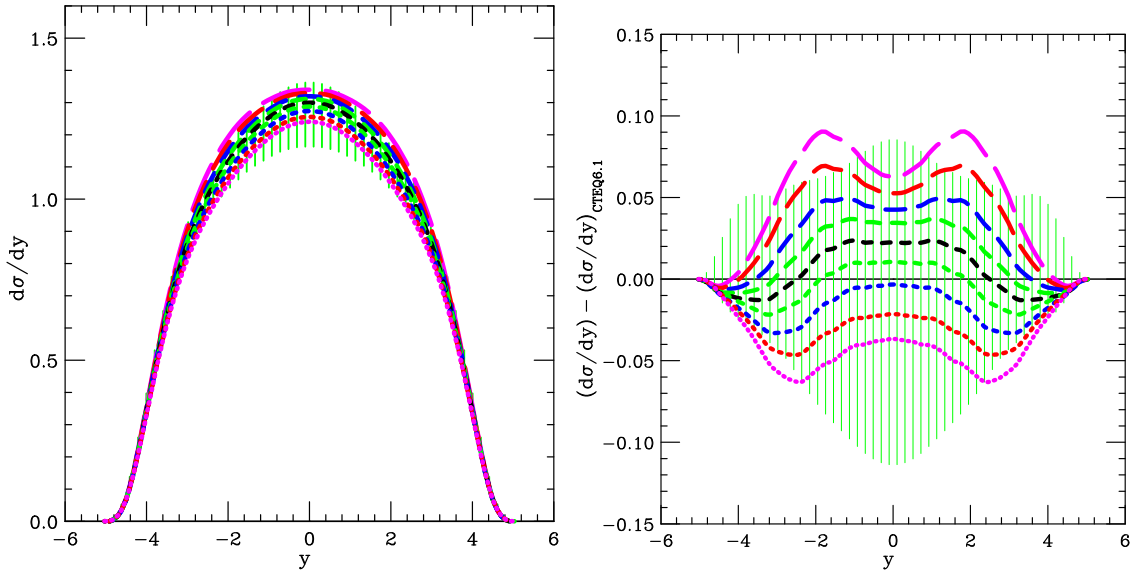

Figure 7: (a) Production of W^- at the LHC; (b) Same process with the CTEQ6.1 prediction subtracted.

the process of W^+ production at the LHC. It has a larger cross section at large rapidity (because $u(x) > d(x)$ for the valence quarks) and a similar range of uncertainty in the prediction. The difference between the central dashed curve and a horizontal line in figures 7 and 8 shows the effect of updates in the fitting between CTEQ6.1 and CTEQ6A118: the change is well within the estimated PDF errors.

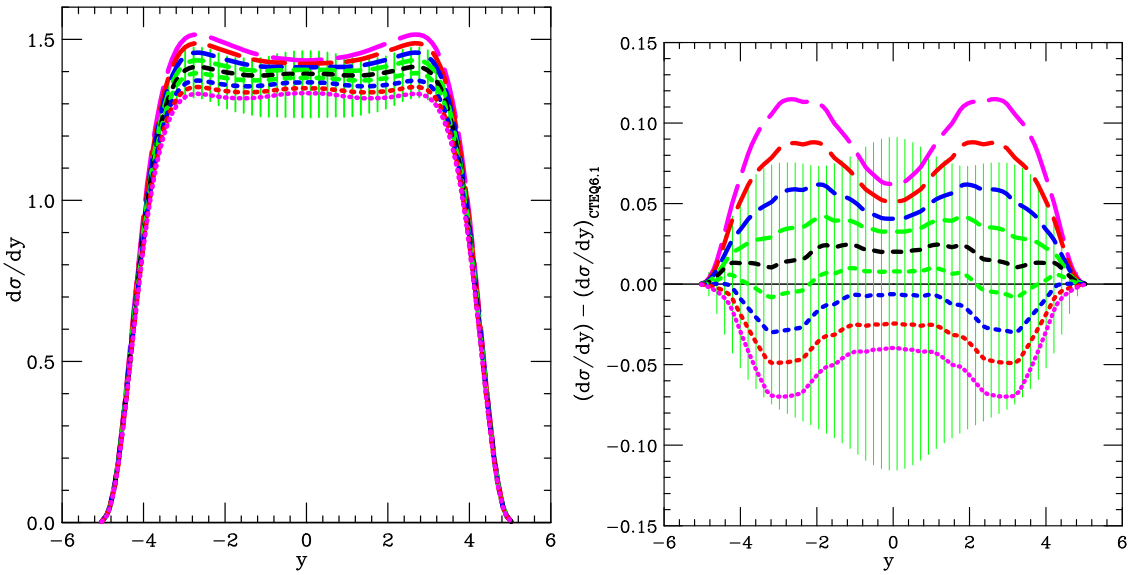

Figure 8: (a) Production of W^+ at the LHC. (b) Same process with the CTEQ6.1 prediction subtracted.

The cross sections for $W^\pm$ production at the LHC are closely tied to the gluon distribution, since the leading-order process in proton-proton collisions is $u + \overline{d} \to W^+$, which involves a sea quark; and sea quarks and the gluon are related at large μ by the evolution equations. (Proton-antiproton collisions at the Tevatron are different because both u and $\overline{d}$ can be valence quarks — which causes the asymmetry in y that can be seen in figure 5.) Also, the next-to-leading order process $u + g \to d + W^+$ involves an initial gluon directly. Hence the predictions for W production at the LHC are somewhat more sensitive to α_s than are the predictions for the Tevatron. Nevertheless, the uncertainty associated with α_s at the LHC, for values of α_s that are consistent with the world average, remains small compared to the other PDF uncertainties as can be seen in figures 7(b) and 8(b).

6.2 Inclusive Jets

Figure 9 shows the α_s-dependence of predictions for inclusive jet production at the Tevatron (in the CDF central rapidity region $0.1 < |y| < 0.7$), and at the LHC (in the region $|y| < 1$). The α_s dependence is exhibited by plotting the ratio of the predicted cross section $d\sigma/dp_T$ to the prediction calculated using CTEQ6.1. As before, the shaded region is the uncertainty range for fixed $\alpha_s(m_Z) = 0.118$ calculated from the eigenvector basis sets of the Hessian approach [10, 20] and the curves show $\alpha_s(m_Z) = 0.110, \ldots, 0.126$.

We observe that if we restrict $\alpha_s(m_Z)$ to a range ± 0.003 which is the 90% confidence range of the world average, the uncertainty due to $\alpha_s(m_Z)$ is small compared to the other PDF uncertainties at large p_T. However, at moderately small p_T the uncertainty in $\alpha_s(m_Z)$ adds considerably to the overall uncertainty for jet production. This comes about because the parton distributions do not depend very strongly on $\alpha_s(m_Z)$ (see figure 3), but the hard cross sections do.

JHEP02(2006)032

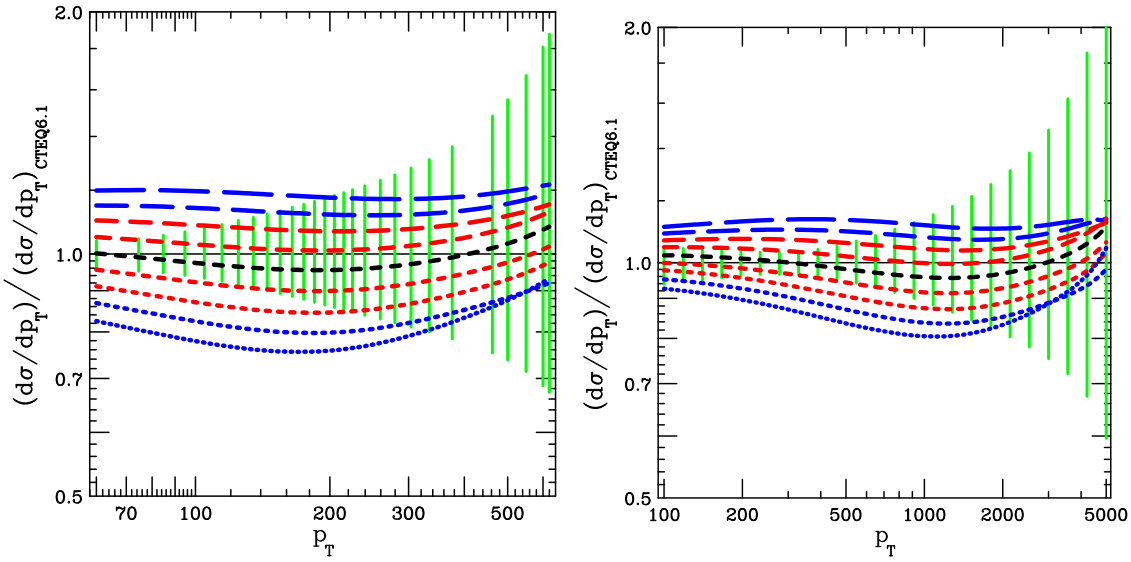

Figure 9: Uncertainties of inclusive jet predictions for Tevatron (a); and LHC (b).

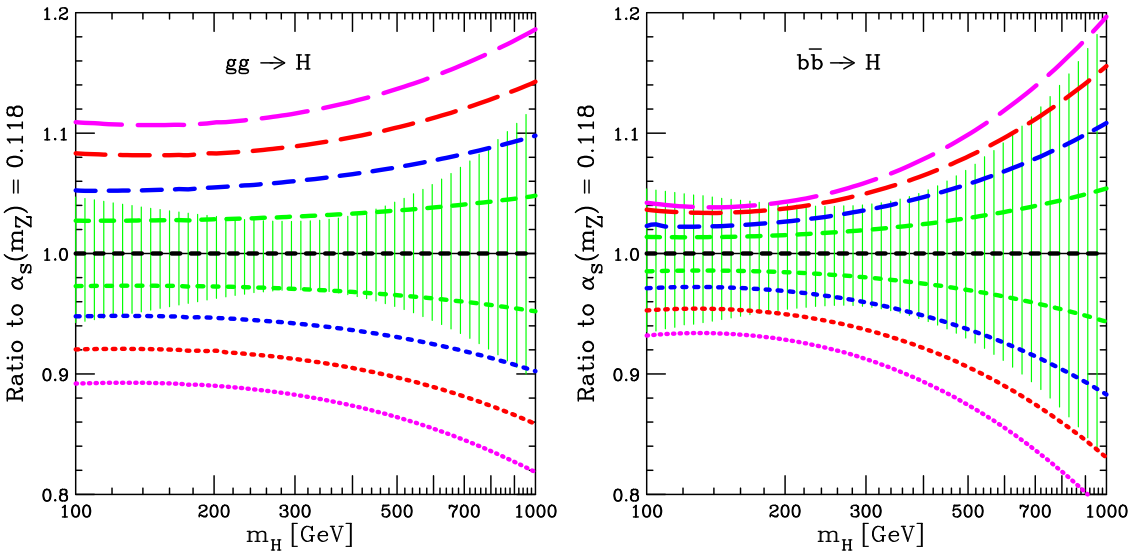

Figure 10: Uncertainty of predictions for Higgs boson production at LHC for the SM and MSSM process $gg \to H$ via top triangle diagram (left); and the MSSM process $b\bar{b} \to H$ (right). Curves (short dash to long dash) show the ratio $\sigma_H(\alpha_s(m_Z))/\sigma_H(0.118)$ for $\alpha_s(m_Z) = 0.110, \ldots, 0.126$. Shaded region shows the uncertainty at $\alpha_s(m_Z) = 0.118$ from other sources.

6.3 Higgs boson cross section in SM and MSSM

The uncertainty of the cross section predicted for Higgs boson production at the LHC as a function of Higgs mass is shown in figure 10. Figure 10(a) shows the uncertainty for the $gg \to H$ process, while figure 10(b) shows the uncertainty for the $b\bar{b} \to H$ mechanism. These cross sections were calculated at NLO using programs from [22, 23] and [24] respec-

tively. Both processes play an important role in Higgs physics: the gg process is dominant in the Standard Model (SM), while in Supersymmetry and some other generic extensions of SM, the $b\bar{b} \to H$ process can be equally important or even dominant. The study of PDF uncertainties is therefore important for both mechanisms of Higgs production.

The uncertainties based on the 40 eigenvector sets of CTEQ6.1 are shown as the shaded regions. These have been shown previously for $gg \to H$ [25] and for $b\bar{b} \to H$ [26]. The 9 curves in each figure show the predictions of the PDF sets with $\alpha_s(m_Z) = 0.110, \ldots, 0.126$ in steps of 0.002 relative to the central value 0.118, which therefore corresponds to the horizontal line at ratio 1.0.

Figure 10(a) shows that the uncertainty in α_s substantially increases the uncertainty in the prediction for $gg \to H$. Particularly for $M_H \simeq 300\,\mathrm{GeV}$ where the non-α_s PDF uncertainty is a minimum, the uncertainty due to α_s is larger than the non-α_s uncertainty. The strong sensitivity of $gg \to H$ to α_s is of course not surprising in view of the α_s^2 dependence coming from the leading order triangle diagram; indeed because the K-factor is large and positive for this process, the NLO corrections make the dependence on α_s even stronger.[6]

Figure 10(b) shows that the contribution of the uncertainty in α_s to $b\bar{b} \to H$ production is comparable to the other PDF uncertainties for that process, so its effect is to add just a modest increase in the overall uncertainty for that process. This is not surprising, since $b\bar{b} \to H$ has no direct dependence on α_s at leading order, and the quark distributions at this momentum scale do not vary rapidly with α_s as seen in figure 10(b).

Figure 11 summarizes the results of figure 10: The dotted curves are the PDF uncertainty at fixed α_s (identical to the boundary of the shaded regions in figure 10) which are intended to show a 90% confidence range. The dashed curve is the uncertainty due to α_s, calculated by interpolation for an uncertainty of $\pm 1.64\,\sigma$ in $\alpha_s(m_Z)$, where $\sigma = 0.002$ from the world average and the factor 1.64 corresponds to a 90% confidence range. The solid curve shows the combined uncertainty obtained by adding the two contributions in quadrature.[7] The additional uncertainty due to α_s is seen to be substantial for the $gg \to H$ process.

7. Conclusion

Previous CTEQ6 parton distributions were extracted from experiment assuming $\alpha_s(m_Z) = 0.118$, based on the world average value. The PDFs presented here were extracted using a

[6] This simple notion agrees quite well quantitatively with the results in figure 10(a). For instance, at $M_H = 100\,\mathrm{GeV}$, raising α_s by 5% from 0.118 to 0.124 would be expected to raise the cross section by about 13%—halfway between 10% (for α_s^2) and 16% (for α_s^3). But meanwhile, $M_H = 100\,\mathrm{GeV}$ requires $x \approx 0.007$, where the increase in α_s causes $g(x)$ to decrease by about 3% according to figure 3(a), which would lower the cross section for $gg \to H$ by 6%. Combining these two effects, the net change is an increase of 7%, which agrees well with the actual increase of 8% that is seen in figure 10(a).

[7] Adding the errors in quadrature, i.e., treating the additional source of error due to $\alpha_s(m_Z)$ as independent of the other PDF errors, is the correct approach according to the Hessian approximation. For in that approximation, $\chi^2 = \chi_0^2 + \sum_i z_i^2$ where the z_i are linear combinations of the PDF shape parameters A_i: $z_i = \sum_j T_{ij} A_j$. When a new parameter such as $(\alpha_s(m_Z) - 0.118)$ is added to the set of fitting parameters, χ_0^2 becomes a quadratic function of that parameter, but there is no change in T_{ij} because in the Hessian approximation one drops all contributions to χ^2 that are higher order than quadratic.

JHEP02(2006)032

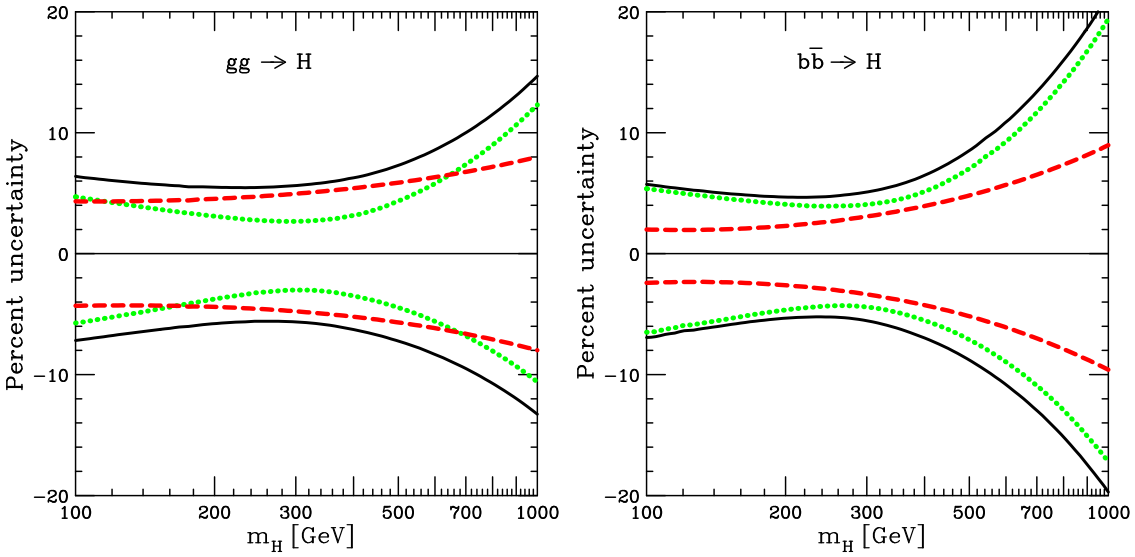

Figure 11: Percentage uncertainty of predictions for Higgs boson production at LHC at 90% confidence. Dashed curves are due to $\alpha_s(m_Z)$ uncertainty; Dotted curves are due to PDF uncertainty at fixed $\alpha_s(m_Z)$; Solid curves are the combined uncertainty.

range of alternative assumptions for $\alpha_s(m_Z)$, using a similar set of experiments with only minor updates.

The new PDFs are named CTEQ6A110, ..., CTEQ6A128, and CTEQ6B110, ..., CTEQ6B128, where the "A" or "B" label indicates the choice of functional form for $\alpha_s(\mu)$ (see section 2) and "110" e.g. indicates $\alpha_s(91.188\,\text{GeV}) = 0.110$. Fortran programs to calculate these PDFs are available at the LHAPDF archive `http://www-spires.dur.ac.uk/HEPDATA/`.

These PDFs can be used to find the range of uncertainty in predictions due to the uncertainty in $\alpha_s(m_Z)$. We find that the previous fits with $\alpha_s(m_Z) = 0.118$ are adequate for most processes, because the uncertainty associated with $\alpha_s(m_Z)$ is smaller than the other sources of PDF uncertainty. However, the $\alpha_s(m_Z)$ uncertainty is important for some predictions that are particularly sensitive to α_s or to the gluon distribution, such as inclusive jet production at relatively small p_T (see figure 9) and Higgs boson production by the $gg \to H$ process in the standard model (see figure 11(a)). This comes about because the intrinsic α_s^2 that is present in the hard scattering processes is only partly compensated by changes in the PDFs with $\alpha_s(m_Z)$ such as those shown in figure 3.

These PDFs can also be used to study the constraints from global fitting or to study individual experiments on the value of $\alpha_s(m_Z)$. In the latter case, the new alpha-series PDFs allow one to take into account the strong correlation between $\alpha_s(m_Z)$ and the gluon distribution that is present at small momentum scales, as shown in figure 2.

Acknowledgments

We thank C.-P. Yuan useful discussions. This research is supported by the National Science Foundation.

JHEP02(2006)032

References

[1] J. Pumplin et al., *New generation of parton distributions with uncertainties from global QCD analysis*, *JHEP* **07** (2002) 012 [hep-ph/0201195].

[2] H.L. Lai et al., *Improved parton distributions from global analysis of recent deep inelastic scattering and inclusive jet data*, *Phys. Rev.* **D 55** (1997) 1280 [hep-ph/9606399].

[3] W.A. Bardeen, A.J. Buras, D.W. Duke and T. Muta, *Deep inelastic scattering beyond the leading order in asymptotically free gauge theories*, *Phys. Rev.* **D 18** (1978) 3998.

[4] Available at the web site http://www.nikhef.nl/~h24/qcdnum.

[5] J. Huston, J. Pumplin, D. Stump and W.K. Tung, *Stability of NLO global analysis and implications for hadron collider physics*, *JHEP* **06** (2005) 080 [hep-ph/0502080].

[6] A.D. Martin, R.G. Roberts, W.J. Stirling and R.S. Thorne, *Uncertainties of predictions from parton distributions, I. Experimental errors*, *Eur. Phys. J.* **C 28** (2003) 455 [hep-ph/0211080].

[7] Particle Data Group collaboration, S. Eidelman et al., *Review of particle physics*, *Phys. Lett.* **B 592** (2004) 1.

[8] A.D. Martin, R.G. Roberts, W.J. Stirling and R.S. Thorne, *MRST2001: partons and α_s from precise deep inelastic scattering and Tevatron jet data*, *Eur. Phys. J.* **C 23** (2002) 73 [hep-ph/0110215].

[9] E.L. Berger, P.M. Nadolsky, F.I. Olness and J. Pumplin, *Light gluino constituents of hadrons and a global analysis of hadron scattering data*, *Phys. Rev.* **D 71** (2005) 014007 [hep-ph/0406143].

[10] D. Stump et al., *Inclusive jet production, parton distributions and the search for new physics*, *JHEP* **10** (2003) 046 [hep-ph/0303013].

[11] BCDMS collaboration, A.C. Benvenuti et al., *A high statistics measurement of the proton structure functions $F_2(x, Q^2)$ and R from deep inelastic muon scattering at high Q^2*, *Phys. Lett.* **B 223** (1989) 485; *A high statistics measurement of the deuteron structure functions $F_2(x, Q^2)$ and R from deep inelastic muon scattering at high Q^2*, *Phys. Lett.* **B 237** (1990) 592.

[12] H1 collaboration, C. Adloff et al., *Measurement of neutral and charged current cross-sections in positron proton collisions at large momentum transfer*, *Eur. Phys. J.* **C 13** (2000) 609 [hep-ex/9908059];
H1 collaboration, C. Adloff et al., *Measurement of neutral and charged current cross sections in electron proton collisions at high Q^2*, *Eur. Phys. J.* **C 19** (2001) 269 [hep-ex/0012052];
Deep inelastic inclusive ep scattering at low x and a determination of α_s, *Eur. Phys. J.* **C 21** (2001) 33 [hep-ex/0012053].

[13] ZEUS collaboration, S. Chekanov et al., *Measurement of the neutral current cross section and f2 structure function for deep inelastic e^+p scattering at HERA*, *Eur. Phys. J.* **C 21** (2001) 443 [hep-ex/0105090].

[14] New Muon collaboration, M. Arneodo et al., *Measurement of the proton and deuteron structure functions, F_2^p and F_2^d and of the ratio σ_L/σ_T*, *Nucl. Phys.* **B 483** (1997) 3 [hep-ph/9610231];
New Muon collaboration, M. Arneodo et al., *Accurate measurement of F_2^d/F_2^p and R^d-R^p*, *Nucl. Phys.* **B 487** (1997) 3 [hep-ex/9611022].

JHEP02(2006)032

[15] CCFR/NuTeV collaboration, U.-K. Yang et al., *Measurements of F_2 and $xF_3^\nu - xF_3^{\bar{\nu}}$ from CCFR ν_μ-Fe and $\bar{\nu}_\mu$-Fe data in a physics model independent way*, *Phys. Rev. Lett.* **86** (2001) 2742 [hep-ex/0009041].

[16] FNAL E866/NuSea collaboration, R.S. Towell et al., *Improved measurement of the $\bar{d}/\bar{u}$ asymmetry in the nucleon sea*, *Phys. Rev.* **D 64** (2001) 052002 [hep-ex/0103030].

[17] CDF collaboration, F. Abe et al., *Search for the decays B_s^0, $B_d^0 \to e^\pm\mu^\pm$ and Pati-Salam leptoquarks*, *Phys. Rev. Lett.* **81** (1998) 5742.

[18] CDF collaboration, T. Affolder et al., *Measurement of the inclusive jet cross section in $\bar{p}p$ collisions at $\sqrt{s} = 1.8$ TeV*, *Phys. Rev.* **D 64** (2001) 032001 [hep-ph/0102074].

[19] D0 collaboration, B. Abbott et al., *Inclusive jet production in $p\bar{p}$ collisions*, *Phys. Rev. Lett.* **86** (2001) 1707 [hep-ex/0011036]; *High-p_T jets in $\bar{p}p$ collisions at $\sqrt{s} = 630$ GeV and 1800 GeV*, *Phys. Rev.* **D 64** (2001) 032003 [hep-ex/0012046].

[20] J. Pumplin et al., *Uncertainties of predictions from parton distribution functions, II. The hessian method*, *Phys. Rev.* **D 65** (2002) 014013 [hep-ph/0101032].

[21] ZEUS collaboration, S. Chekanov et al., *A zeus next-to-leading-order QCD analysis of data on deep inelastic scattering*, *Phys. Rev.* **D 67** (2003) 012007 [hep-ex/0208023].

[22] M. Spira, A. Djouadi, D. Graudenz and P.M. Zerwas, *Higgs boson production at the LHC*, *Nucl. Phys.* **B 453** (1995) 17 [hep-ph/9504378].

[23] M. Spira, *Higlu and hdecay: programs for Higgs boson production at the LHC and Higgs boson decay widths*, *Nucl. Instrum. Meth.* **A389** (1997) 357 [hep-ph/9610350].

[24] C. Balazs, H.-J. He and C.P. Yuan, *QCD corrections to scalar production via heavy quark fusion at hadron colliders*, *Phys. Rev.* **D 60** (1999) 114001 [hep-ph/9812263].

[25] A. Djouadi and S. Ferrag, *Pdf uncertainties in Higgs production at hadron colliders*, *Phys. Lett.* **B 586** (2004) 345 [hep-ph/0310209].

[26] A. Belyaev, J. Pumplin, W.-K. Tung and C.P. Yuan, *Uncertainties of the inclusive Higgs production cross section at the Tevatron and the LHC*, *JHEP* **01** (2006) 069 [hep-ph/0508222].

JHEP02(2006)032